RSC Advances

ROYAL SOCIETY OF CHEMISTRY

www.rsc.org/advances

1 **Preparation of liquefied wood-based activated carbon fibers by different activation**

2 **methods for methylene blue adsorption**

3 Yuxiang Huang, Erni Ma, Guangjie Zhao[*]

4 College of Materials Science and Technology, Beijing Forestry University, Tsinghua

5 East Road 35, Haidian 100083, Beijing, China

6 **Abstract**

7   In order to study the adsorption for methylene blue (MB), five types of activated

8 carbon fibers (ACFs) were prepared from liquefied wood by different activation

9 methods. The ACFs activated by pure physical and chemical activation were dominantly

10 microporous and mesoporous, respectively, which showed relatively low adsorption

11 capacity for MB. The chemical/physical coupling activation was an effective method to

12 improve the mesoporosity resulting in the reinforcement of MB adsorption ability. ACFs

13 by chemical-physical reactivation even had abundant macropores in addition to

14 well-developed micro- and mesoporosity, while physical-chemical reactivation did not

15 seem to be an efficient one. Their potentially different mechanisms of pore formation

16 and kinetics adsorption of MB were investigated.

17 **Keywords:** Activated carbon fibers; liquefied wood; activation methods; methylene

18 blue adsorption; kinetics

19 **1. Introduction**

20   Dyes have been widely applied in many industries, such as textile, paper

21 production, food technology, etc[1]. The attendant industrial wastewater usually contains

22 a great deal of organic compounds and toxic substances. For example, methylene blue

23 (MB), commonly used for dying cotton, wood and silk, is harmful to people's eyes and

24 inhalation that it can cause eye burns and give rise to short periods of difficult

---

[*] Corresponding author. Tel: 86 10 62338358.   E-mail: zhaows@bjfu.edu.cn (Guangjie Zhao)

1   breathing[2-4]. Besides, ingestion via the mouth would result in a burning sensation and

2   may cause other diseases such as nausea, mental confusion and painful

3   micturition[5].Thus, the treatment of wastewater consisting mostly of such dye is of great

4   importance.

5   Activated carbon fibers (ACFs), due to their capability for efficiently adsorbing a

6   broad range of adsorbates and their simplicity of design, have been found to be superior

7   to other techniques for wastewater treatment[1]. However, most of them are prepared

8   from fossil resources such as coals, which are not only expensive but also

9   non-renewable. Currently, renewable industrial and agricultural by-products such as

10   liquefied wood used as precursors have attracted more and more attentions on account

11   of their advantages in environmental protection and regeneration[6-7].

12   In our laboratory, ACFs of specific surface area more than 2000m^2/g were prepared

13   from liquefied wood by steam activation[8] , but these microporous ACFs were not

14   suitable for adsorption of large molecule substance like MB. In our previous work,

15   ACFs with mesoporosity by KOH activation were prepared and reaction mechanisms

16   during the activation were investigated[9]. Hence, an attempt was made here to combine

17   the two methods either simultaneously or separately to promote the generation of

18   mesoporosity and even macroposity for large molecule substance's adsorption. The

19   mechanisms on pore formation during activation process as well as the adsorption

20   isotherm and kinetics of the obtained ACFs were investigated.

21   **2. Experimental**

22   *2.1 Preparation and characterization of ACFs*

23   Liquefied wood-based fibers were prepared through a series of process including

24   liquefaction, melt-spinning and curing according to our previous study[10], based on

25   which five activation methods were employed to prepare ACFs (Fig. 1). All the ACFs

1   were washed with hot deionized water and 0.1 M hydrochloric acid until the pH of the

2   washing solution reached 6-7. The porosity changes were observed by a scanning

3   electron microscope (SEM, Hitachi S-3400N, Japan) coupled with an energy dispersed

4   X-ray analyzer (Horiba 7021-H, Japan) and analyzed by N_2 adsorption at 77K

5   (Quantachrome, Autosorb-iQ, USA). The chemical groups of the samples were studied

6   by a Fourier transform infrared spectrometer (FTIR, BRUKER Tensor 27, German) in

7   the range of 4000-400 cm^{-1}, using pellets with samples dispersed in KBr. X-ray

8   photoelectron spectroscopy (XPS) measurements were carried out on a

9   spectrophotometer (Thermo Scientific ESCALAB 250Xi) to determine the number of

10   functional groups present on the surface of the ACFs with a monochromated Al Ka

11   X-ray source (hv = 1486.6 eV) and a nonlinear least squares curve-fitting program

12   (XPSPEAK software, Version 4.1) was employed for XPS spectral deconvolution. The

13   determination of the pH_{pzc} of the ACFs was carried out by using the acid base titration

14   reported by Bouaiz et al. (2015)[11]. 10ml NaCl solution (0.01M) with pH value between

15   2 and 12 (adjusted using either HCl or NaOH, 0.1M) was added to 30 mg of ACFs and

16   the final pH measured after 24h under agitation at room temperature. The pH is the

17   point where the curve pH_{final} vs. pH_{inital} crosses the line $pH_{initial}=pH_{final.}$

18   *2.2 Adsorption experiments*

19   The adsorption performance of the as-prepared ACFs was tested for the adsorption

20   of methylene blue (MB, CAS 7220-79-3, Tianjin Jinke Fine Chemicals CO. Ltd., China).

21   The tests were performed in a set of Erlenmeyer flasks (100 mL) where 100 ml of MB

22   solutions with initial concentrations of 100-500 mg/L were placed in these flasks. About

23   3 mg of ACFs was added to each flask and kept in an isothermal shaker at 25 ^{o}C for 24

24   h to reach equilibrium. Aqueous samples were taken from the solutions and the

25   concentrations were analyzed. Prior to analysis, all samples were filtered in order to

1 minimize interference of carbon fines with the analysis. The concentrations of MB in

2 the supernatant solutions before and after adsorption were determined by using a UV-vis

3 spectroscopy (Biowave II, WPA, England) at a wavelength of 665nm. The adsorbed MB

4 mass per unit mass, q_t (mg/g) at adsorption time t (h) was calculated by:

5 $$q_t = \frac{(C_0 - C_t)V}{m} \tag{1}$$

6 Where C_0 (mg/L) and C_t (mg/L) are the liquid-phase concentrations of dye at initial

7 time t (h) the initial MB concentration. V is the volume of solution (L) and m is the

8 mass of the adsorbent.

9 **3. Results and discussion**

10 *3.1 Textural characterization of prepared ACFs*

11 *3.1.1 Yield of ACFs*

12   Basically, ACFs of high specific surface area are associated with low yield. An

13 efficient ACF production process combines a well-developed porosity with an

14 acceptable fabrication yield. In the present study, the ACF production yields were

15 monitored for the five activation methods.

16   As shown in Table 1, there is a difference in the yield as a function of the

17 activating agent for the same activating temperature. The yield of ACFs by single KOH

18 activation (K1) was as high as 76%, while the yield of ACFs by single steam activation

19 (S1) was 41%, suggesting the latter had a better porosity development. For the case of

20 chemical/physical activation (KS), physical-chemical (S1K2) and chemical-physical

21 reactivation (K1S2), the ACF production yields were quite similar (26%, 27% and 30%,

22 respectively), which had a significant reduction compared with those of ACFs by single

23 activation. This can be attributed to the additional activation process that resulted in

24 more burn-off of carbon.

25 *3.1.2 Nitrogen adsorption behavior and porosity development*

1   Fig. 2 shows the adsorption/desorption isotherms of N_2 for the ACFs prepared by

2   different activation methods. The shape of the isotherm curves was analyzed sing the

3   IUPAC classification[12]. The isotherms for S1 and S1K2 belong to type I based on the

4   IUPAC classification that rose sharply at low relative pressures and approached a

5   plateau which was parallel to the relative pressure axis, indicating these ACFs were

6   mainly microporous. The N_2 uptake of S1 is higher than that of S1K2, meaning that

7   reactivation with KOH reduced the pore volume. However, for the K1, the absorbed

8   volume maintains a linear upward trend from very low pressure even less than 0.1,

9   indicating the isotherms belonged to non-microporous type. The isotherms of KS and

10   K1S2 are characterized by both a broader knee and a clearer hysteresis loop,

11   corresponding to a combination of type I and IV isotherm[13], suggesting the co-existence

12   of micropores and mesopores. Meanwhile, a small tail can be observed at the end of

13   isotherms, implying the appearance of macropores.

14   The pore size distributions (PSDs) of the ACFs obtained by applying Density

15   Functional Theory (DFT) method to N_2 adsorption data are presented in Fig. 3 and their

16   pore structure parameters are summarized in Table 1. The PSDs of S1 and S1K2 mainly

17   concentrate in micropore region where the contour of their PSDs are very similar, but

18   micropore accumulation of S1K2 is lower than that of S1 (Fig.3 a). And mesopore

19   accumulation of S1K2 has a slight decrease rather than an anticipated increase, except

20   for the peak at *ca.* 6.8nm. This states that reactivation with KOH did not produce

21   mesoporosity but reduced the microporosity on the contrary. The possible reaction

22   between KOH and carbon could be described as follows:

23   $6KOH + 2C \rightarrow 2K + 3H_2 + 2K_2CO_3$ (2)

24   It can be inferred that, after impregnation, KOH mainly concentrated in the micropores

25   which were created by single steam activation. The concentration of evolved H_2 would

1   reach very high value due to the confined space (Fig .4a), which could inhibit the

2   forward reaction (1)[14]. Thus, KOH cannot efficiently serve as an activator. Furthermore,

3   the remaining KOH and reaction products such as K_2CO_3 blocked the pores and

4   decreased microporosity. This phenomenon was very similar to the result of Miyamoto

5   et al. (2005)[15], who produced ACFs by K_2CO_3 reactivation from pith-based ACFs. Their

6   result showed reactivation with K_2CO_3 did not produce mesoporosity and reduced the

7   microporosity.

8   As for K1, there are few micro- and mesopores mainly accumulate in a narrow

9   range around 2-4nm and 5-10nm, indicating that KOH helped to produce mesopores

10   when the concentration of KOH solution was low (10%). When K1 was reactivated to

11   K1S2, microporosity had a great development. In addition, mesopores accumulated to a

12   deeper extent and macropore volume had a sharp increase simultaneously. This can be

13   interpreted that carbon atom at the graphite layers was further eroded by steam during

14   the reactivation. This process resulted in the formation of dominant micropores and

15   contributed to the enlargement of some micro- and mesopores into meso- and

16   marcopores, respectively (Fig. 4b). Relatively speaking, pure KOH activation is width

17   activation for mesopore formation, while steam reactivation can be recognized as depth

18   activation which is responsible for micropore generation and of pore expansion.

19   Compared with K1 and K1S2, KS has similar PSDs but presents more mesopore

20   accumulation around 2-15nm, and the macropore volume falls in the range between K1

21   and K1S2. This phenomenon can be ascribed to several reasons as follows. During the

22   coupling activation, when the temperature reached the activation temperature (1123K),

23   a little KOH attached on the fibers had already reacted with carbon, thereby some

24   mesopores formed. The introducing of steam improved the micropore reaction and this

25   steam flow could decrease the intra-pore gas phase concentrations, thereby promoting

1   the reaction between KOH and carbon to generate mesopores. Furthermore, less

2   reaction points were provided for steam activation compared with reactivation process

3   of K1S2 (Fig. 4c) owing to parts of the fiber surface taken up by KOH as well as the

4   effect of the evolved H_2 flow. Therefore, less mesopores could be enlarged to

5   macropores. Accordingly, the corresponding micropore accumulation of KS should be

6   lower than that of K1S2. This is just verified by the data of micropores in Table 1.

7

8   *3.1.3 Chemical structure characteristics*

9   The 4000-400 cm^{-1} infrared spectral region of the liquefied wood-based ACFs

10 prepared by different activation methods is shown in Fig. 5. The spectra of S1 and K1

11 exhibit similar bands and shoulders which are assigned to various vibration modes in

12 atomic groups and structures except two peaks in 1300-1000 cm^{-1} region, where the

13 band is quite difficult to be identified because it may be ascribed to C-O in acids,

14 alcohols, phenols, ethers or ester groups[16]. The peaks at 1089 and 1049 cm^{-1} in the

15 spectrum of K1 indicated various types of C-O groups existed in KOH-activated ACFs.

16 Nevertheless, the two peaks become weak in the spectra of K1S2, S1K2 and KS,

17 suggesting the decrease of oxygen containing functional groups caused by further or

18 coupling activation. Moreover, two bands at 880 and 798 cm^{-1} appear in the spectrum of

19 each sample, which are attributed to the out-plane bending vibration of C-H in the

20 aromatic rings[17]. This demonstrated low substituted aromatic rings still existed in the

21 structure of these ACFs.

22   The elemental compositions of the ACFs by EDX are listed in Tabel 2. Basically,

23 the oxygen content of ACFs by reactivation or coupling activation had a slight decrease

24 compared to those by single activation. However, it is noteworthy that the oxygen

25 content of S1K2 is even higher than any other ACFs, which is in agreement with the

1   above porosity analysis. It can be attributed to the high concentration of KOH in the

2   micropores by using this reactivation method. The XPS analysis was further used to

3   evaluate the changes in the chemical bonding states and concentrations of the surface

4   functional groups. For all ACF samples, the C1s signals exhibited an asymmetric tailing

5   (Fig. 6), which was partially due to the intrinsic asymmetry of the graphite peak or to

6   the contribution of oxygen surface complexes. Thus, the C1s spectrum has been

7   deconvoluted into six components with binding energies corresponding to: (I) graphite

8   type (284.7 eV); (II) amorphous carbon present in phenol, alcohol, ether or C=N groups

9   (285.6-285.8 eV); (III) carbonyl or quinine groups (286.6-286.9 eV); (IV) carboxyl,

10 lactone, or ester groups (287.7-289.9 eV); (V) carbonate groups (289.3-290.9 eV) and

11 (VI) a peak corresponding to $\pi=\pi^*$ transitions in aromatic rings (291.3-291.7 eV)[18].

12 These functional groups might exercise a profound impact on the surface properties of

13 ACFs and thus affected their adsorption characteristics.

14 *3.2 Equilibrium and kinetics adsorption of ACFs*

15   From Table 2, the pH_{pzc} values of all the ACFs were found to be 6-7, which

16 indicated that the surface of the ACFs were nearly neutral. The original pH of the MB

17 solution was found to be 6.6, which is above the pH_{pzc} of the ACFs. According to

18 previous literature, at $pH>pH_{pzc}$, the ACFs' surfaces are negatively charged favouring

19 the adsorption of cationic dyes such as MB[11]. Therefore, this pH of the MB solution was

20 very suitable for higher removal from aqueous solution.

21 *3.2.1 Effect of contact time and initial MB concentration on adsorption equilibrium*

22   Fig. 7 shows the adsorption capacity of the ACFs versus the adsorption time at

23 various initial MB concentrations at 25 $^{\circ}$C, where the amount of adsorbed MB increases

24 with time until reaching a plateau phase for all concentrations. Nevertheless, the contact

25 time needed for MB solution to reach equilibrium varies according to the initial MB

1   concentration. As for the lower concentrations (i.e. 100 and 200 mg/L), about 5 h were

2   necessary to reach equilibrium while 12 h were required for the higher concentrations

3   (300-500 mg/L). According to previous literature[1], the mass transport associated with

4   the adsorption of solute form solution by porous adsorbent was divided into three steps

5   including the adsorbate migrating through the solution, solute movement from particle

6   surface into interior site and adsorbate being adsorbed into the active sites at the interior

7   of the adsorbent particle, which takes relatively long contact time. A similar

8   phenomenon was observed for the adsorption of dyes onto ACs from Mediterranean

9   *Posidonia oceanica* (L.) fibers[19] and the equilibrium time was 8-10 h for higher MB

10   concentrations.

11   The amount of dye adsorbed at the equilibrium time reflects the maximum

12   adsorption capacity of the adsorbent under those operating conditions. The adsorption

13   capacity of KS at equilibrium (q_e) (obtained by q_t at 24 h) increased from 234 to 920

14   mg/g with increasing the initial concentrations from 100 to 500 mg/L. This can be

15   attributed to the increase in the concentration gradient or higher concentration of MB in

16   solution which leads to enhanced adsorption capacity of ACFs, further being conformed

17   by the Le Chatelier's principle which suggests that equilibrium position shifts towards

18   adsorption with the increment in adsorbate concentration in solution. As seen from

19   Table 1, under the same initial concentrations (500 mg/L) and operating conditions, KS

20   shows the highest capacity for MB followed by K1S2. K1 has a MB adsorption amount

21   of 684 mg/g, while S1 only exhibits 242 mg/g, demonstrating that physical-chemical

22   reactivation or chemical/physical coupling activation really improved the adsorption

23   ability for MB. S1K2 with the lowest V_{meso} also presents the weakest adsorption

24   properties, indicating MB adsorption was strongly related to V_{meso}.

25   *3.2.2 Adsorption isotherms*

1   The adsorption isotherm is fundamentally helpful to describe how adsorbates

2   interact with adsorbents and how the adsorption molecules distribute between the liquid

3   phase and solid phase when the adsorption process reaches an equilibrium state[20].

4   Therefore, it is critical in optimizing the use of adsorbents. In this work, both of the

5   Langmuir and the Freundlich equations[21] were adopted to isotherm data fitting for the

6   adsorption of MB onto the ACFs. The applicability of the two models was compared by

7   judging the correlation coefficients (R^2), which are recorded in Table 3.

8   From Table 3, the Langmuir isotherm model yielded better fit with the higher R^2

9   value than the Freundlich model. The value of R_L, a dimensionless equilibrium

10   parameter which expressed as the essential characteristics of the Langmuir isotherm[21], is

11   found to be 0.0018-0.0029, falling in the favorable range of 0-1, and this again

12   confirmed that the Langmuir model was favorable for adsorption of MB onto the

13   liquefied wood-based ACFs, implying the homogeneous nature of ACF surface and the

14   adsorption of MB onto liquefied wood-based ACFs was monolayer adsorption.

15   *3.2.3 Adsorption kinetics*

16   Adsorption kinetics is capable to provide information about the mechanism of

17   adsorption and potential rate controlling steps such as mass transfer and chemical

18   reaction, which is important for designing a fast and effective model adsorption system

19   in practice[22], so three simplified kinetic models including pseudo-first-order[23],

20   pseudo-second-order[24] and intraparticle diffusion model[25] were applied to investigate

21   the mechanism of the adsorption process. Based on the adsorption data of KS, these

22   three kinetics models were plotted in Fig. 8 and all the calculated parameters are

23   summarized in Table 4. It was found that all of the correlation coefficients are greater

24   and the sum of error squares (SSE) are smaller for pseudo-second-order kinetic model

25   compared to those for the other two kinetics. It also showed a good agreement between

the experimental and the calculated q_e values in case of pseudo-second-order kinetics,

indicating the kinetic adsorption behavior of MB onto liquefied wood-based ACFs can

be favorably described by pseudo-second-order model.

4. Conclusions

The porosity of ACFs could be designed and well controlled for MB adsorption by

different combination scheme of physical and chemical activation, which was probably

attributed to different mechanisms on pore formation. Because KOH activation

provided more reaction points for the subsequent steam activation, ACFs rich in

macropores with developed micro- and mesoporosity can be prepared by steam-KOH

reactivation and showed excellent adsorption ability, which was not true if the two-step

activation was reversed. Chemical/physical coupling activation is also an effective

method to improve MB adsorption capacity as a result of enhancing mesoporosity as

well as ensuring high specific surface area. Equilibrium data were fitted to Langmuir

and Freundlich isotherms and the former was seemed to be better. The kinetics of the

adsorption process was found to follow the pseudo-second-order kinetic model.

References

1 I. A.W. Tan, B.H. Hameed and A.L. Ahmad, Equilibrium and kinetic studies on basic

dye adsorption by oil palm fibre activated carbon, *Chem. Eng. J.*, 2007, 127,

111-119.

2 D. Ghosh and K.G. Bhattacharyya, Adsorption of methylene blue on kaolinite, *Appl.

Clay Sci.*, 2002, 20, 295-300.

3 B.H. Hameed, A.T.M. Din and A.L. Ahmad, Adsorption of methylene blue onto

bamboo-based activated carbon: Kinetics and equilibrium studies, *J. Hazard. Mater.*, 2002, 141, 819-825.

4 A.F. Hassan, A.M. Abdel-Mohsen and Moustafa M.G. Fouda, Comparative study of calcium alginate, activated carbon, and their composite beads on methylene blue adsorption, *Carbohydr. Polym.*, 102, 192-198.

5 J. Avom, J.K. Mbadcam, C. Noubactep and P. Germain, Adsorption of methylene blue from an aqueous solution onto activated carbon from palm-tree cobs, *Carbon*, 1997, 35, 365–369.

6 M.E. Fernandez, G.V.N. Pablo, P.R. Bonelli and A.L. Cukierman, Activated carbon developed from orange peels: Batch and dynamic competitive adsorption of basic dyes, *Ind. Crops Prod.*, 2014, 43, 617-622.

7 X. Ma, F. Zhang and J. Zhu, Preparation of highly developed mesoporous activated carbon fiber from liquefied wood using wood charcoal as additive and its adsorption of methylene blue from solution, *Bioresour. Technol.*, 2014, 164, 1-6.

8 W. Liu and G. Zhao, Effect of temperature and time on microstructure and surface functional groups of activated carbon fibers prepared from liquefied wood, *BioResources*, 2012, 4, 5552-5567.

9 Y. Huang, E. Ma and G. Zhao, Thermal and structure analysis on reaction mechanisms during the preparation of activated carbon fibers by KOH activation from liquefied wood-based fibers, *Ind. Crops Prod.*, 2015, 69, 447–455.

10 Y. Huang and G. Zhao, Preparation and characterization of activated carbon fibers from liquefied wood by KOH activation, *Holzforschung*, 2015, Online.

11 F. Bouaziz, M. Koubaa, F. Kallel, F. Charri, D. Driss, R.E. Ghorbel, and S.E. Chaabouni, Efficiency of almond gum as a low-cost adsorbent for methylene blue dye removal from aqueous solutions, *Ind. Crops Prod.*, 2015, 74, 903-911.

12 K.S.W. Sing, D.H. Everett, R.A.W. Haul, L. Moscou, R.A. Piepotti, J. Rouquérol and T. Siemieniewska, Reporting physisorption data for gas/solid systems with special reference to the determination of surface area and porosity, *Pure Appl. Chem.*, 1985, 57, 603–619.

13 X. Du, W. Zhao, Y. Wang, C. Wang, M. Chen, T. Qi, C. Hua and M. Ma, Preparation of activated carbon hollow fibers from ramie at low temperature for electric double-layer capacitor applications, *Bioresour. Technol.*, 2013, 149, 31-37.

14 D. Lozano-Castelló, J.M. Calo, D. Cazorla-Amorós and A. Linares-Solano, Carbon activation with KOH as explored by temperature programmed techniques, and the effects of hydrogen, *Carbon*, 2007, 45, 2529－2536.

15 J. Miyamoto, H. Kanoh, and K. Kaneko, The addition of mesoporosity to activated carbon fibers by a simple reactivation process. Carbon, 2005, 43, 855-857.

16 M. Benadjemia, L. Millière, L. Reinert, N. Benderdouche and L. Duclaux, Preparation, characterization and Methylene Blue adsorption of phosphoric acid activated carbons from globe artichoke leaves, *Fuel Process. Technol.*, 2011, 92, 1203 - 1212.

17 J.C. Domínguez, M. Oliet, M.V. Alonso, E. Rojo and F. Rodríguez, Structural, thermal and rheological behavior of a bio-based phenolic resin in relation to a commercial resol resin, *Ind. Crops Prod.*, 2013, 42, 308-314.

18. X. Ma, F. Zhang, L. Wei, Effect of wood charcoal contents on the adsorption property, structure, and morphology of mesoporous activated carbon fibers derived from wood liquefaction process, *J. Mater. Sci.*, 2015, 50, 1908-1914.

19 M.C. Ncibi, R. Ranguin, M.J. Pintor, V. Jeanne-Rose, M. Sillanp, S. Gaspard, Preparation and characterization of chemically activated carbons derived from Mediterranean Posidonia oceanica (L.) fibres, *J. Anal. Appl. Pyrolysis*, 2015, 109,

205 - 214.

20 R. Yang, G. Liu, X. Xu, M. Li, J. Zhang and X. Hao, Surface texture, chemistry and adsorption properties of acid blue 9 of hemp (Cannabis sativa L.) bast-based activated carbon fibers prepared by phosphoric acid activation, *Biomass Bioenergy*, 2011, 35, 437-445.

21 T.W. Weber and R.K. Chakravorti, Pore and solid diffusion models for fixed‐bed adsorbers, *AlChE J.*, 1974, 20, 228-238.

22 S. Senthikumaar, P.R. Varadarajan, K. Porkodi and C.V. Subbhuraam, Adsorption of methylene blue onto jute fiber carbon: kinetics and equilibrium studies. *J. Colloid Interface Sci.*, 2005, 284, 78-82.

23 S. Langergren, and B.K. Svenska, Zur Theorie der sogenannten Adsorption gelöster Stoffe, *Veternskapsakad Handlingar*. 1989, 24, 1-39.

24 Y.S. Ho and G. McKay, Sorption of dye from aqueous solution by peat, *Chem. Eng. J.*, 1988, 70, 115-124.

25 K.K.H. Choy, J.F. Porter and G. Mckay, Intraparticle diffusion in single and multicomponent acid dye adsorption from wastewater onto carbon. *Chem. Eng. J.*, 2004, 103, 133-145.
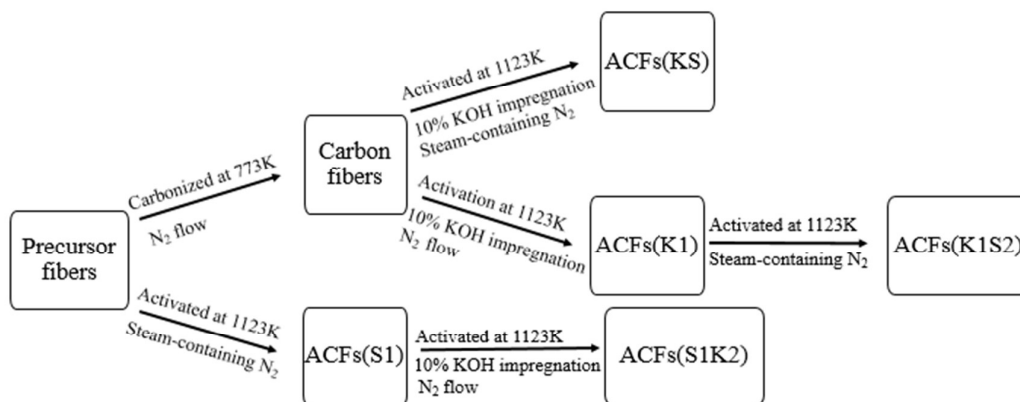
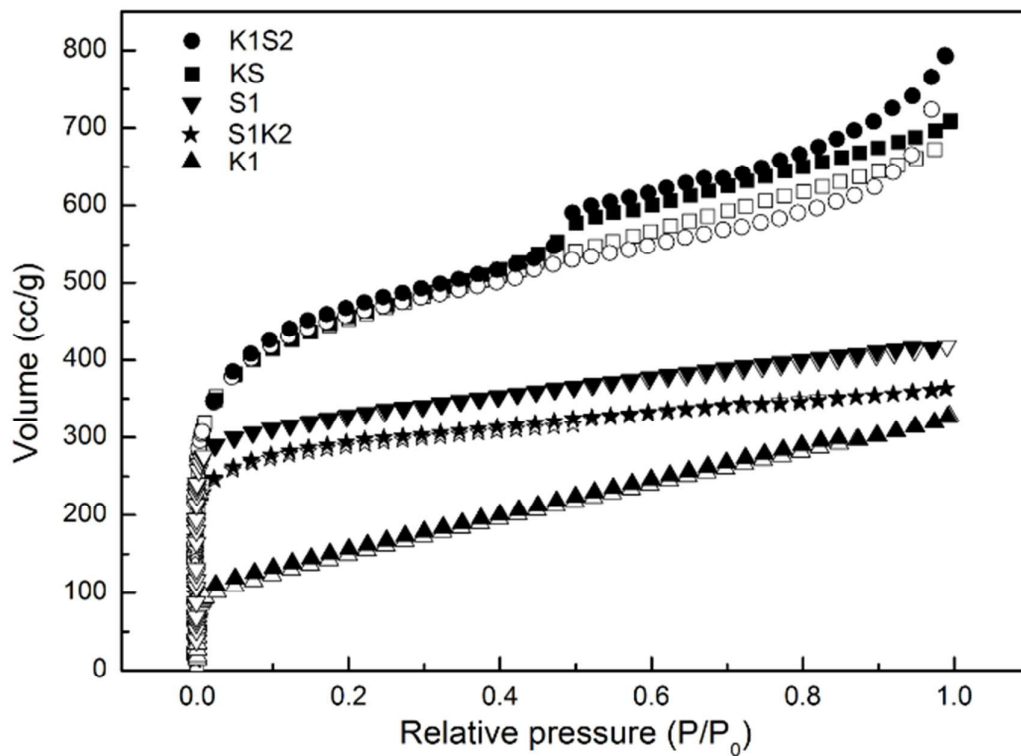Fig. 1. Scheme of process routes for preparing ACFs by different activation methods.

Fig. 2. N$_2$ adsorption isotherms for the ACFs. Open symbols: adsorption branch. Solid symbols: desorption branch.
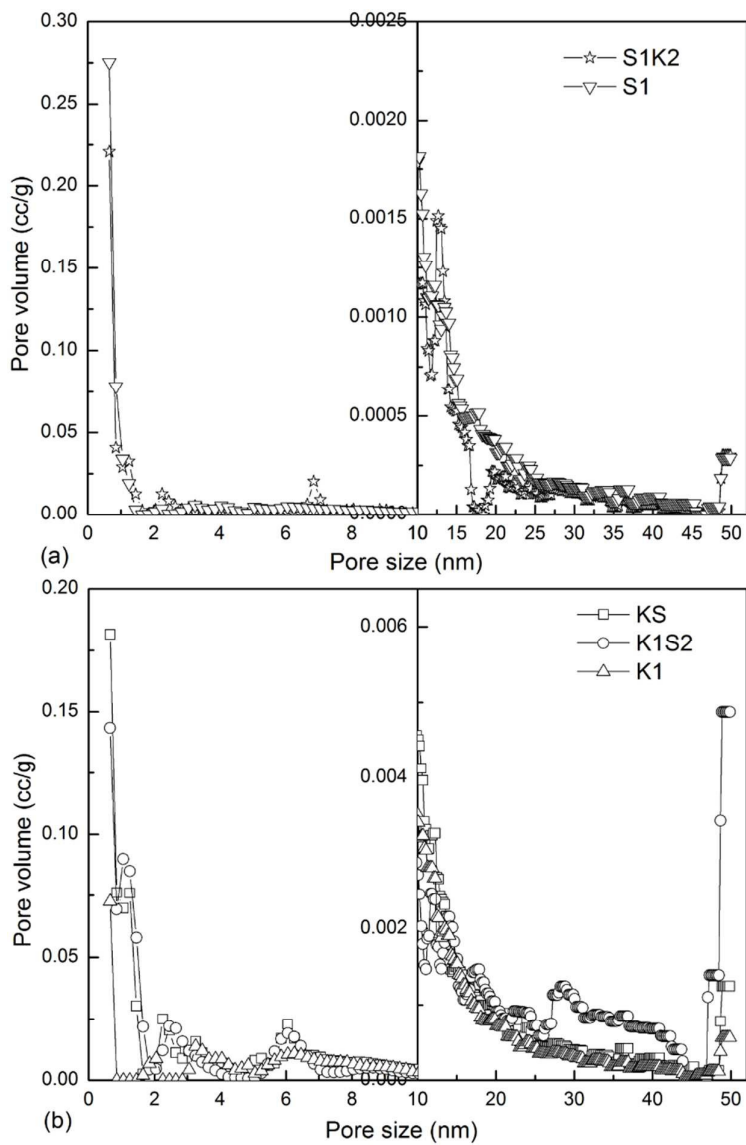
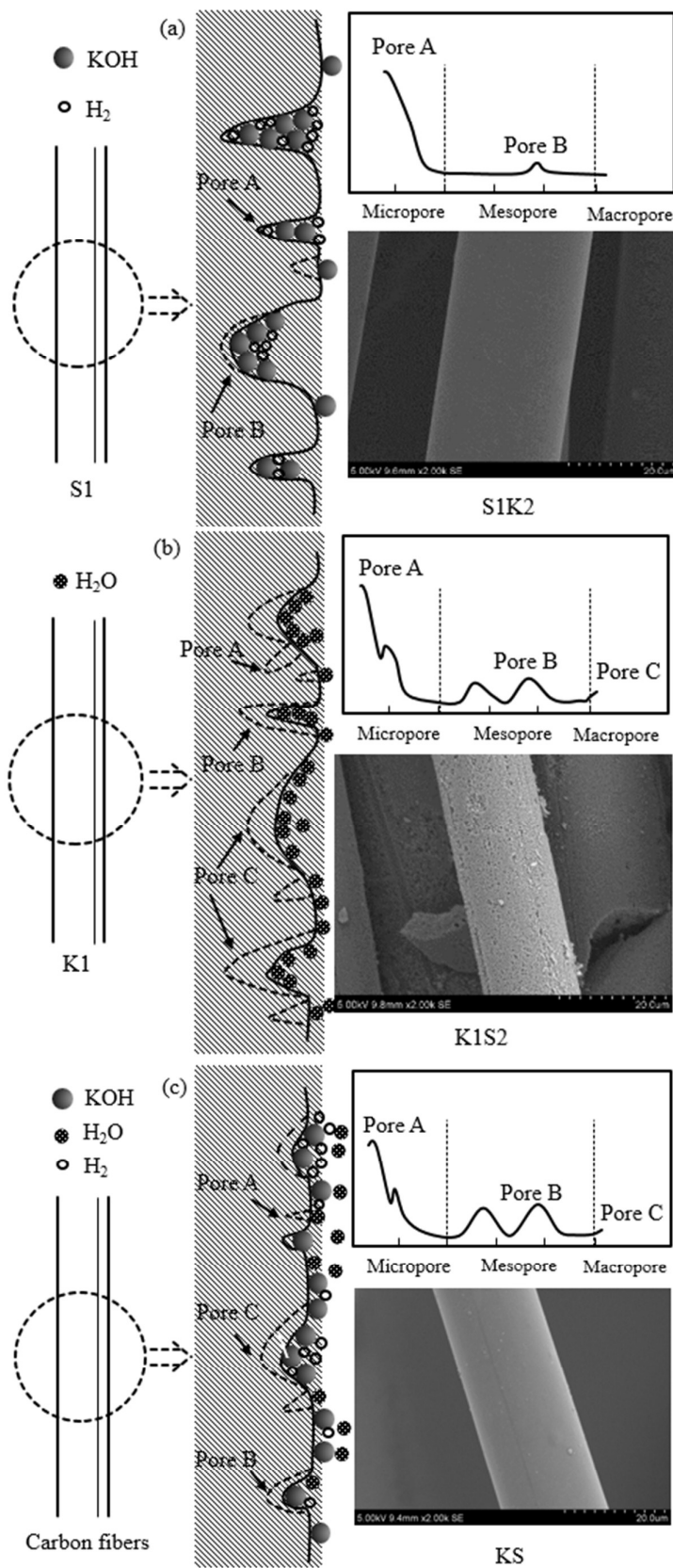Fig. 3. DFT pore size distributions for the ACFs.

Fig. 4. Possible mechanisms of pore formation during the reactivation and coupling activation.
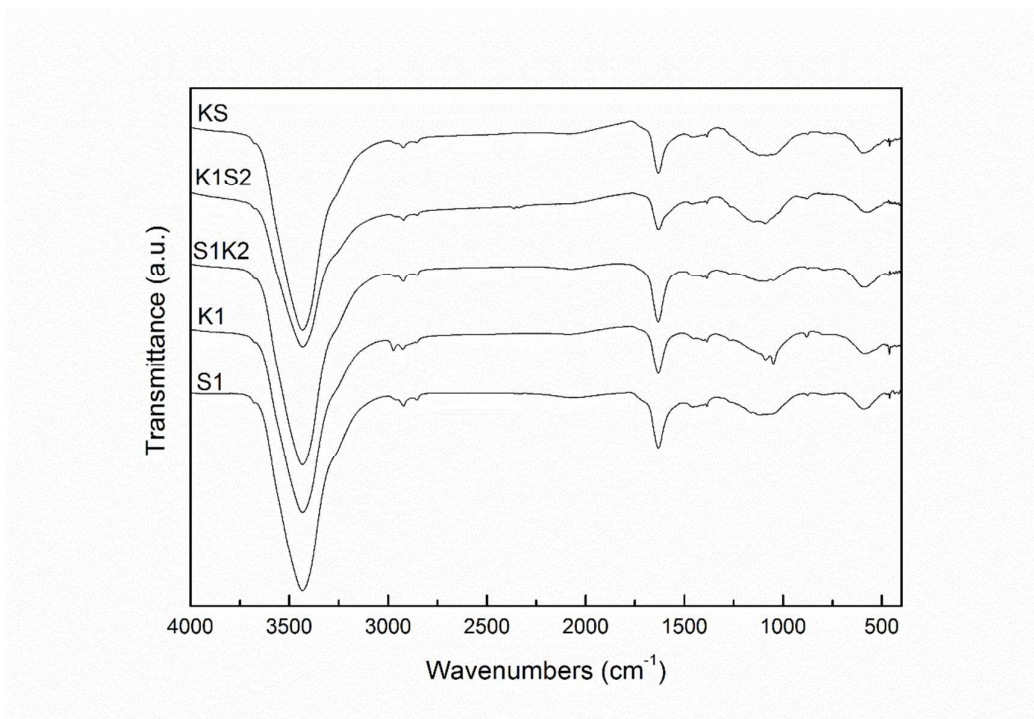
Fig. 5. FTIR spectra of liquefied wood-based ACFs prepared by different activation methods.
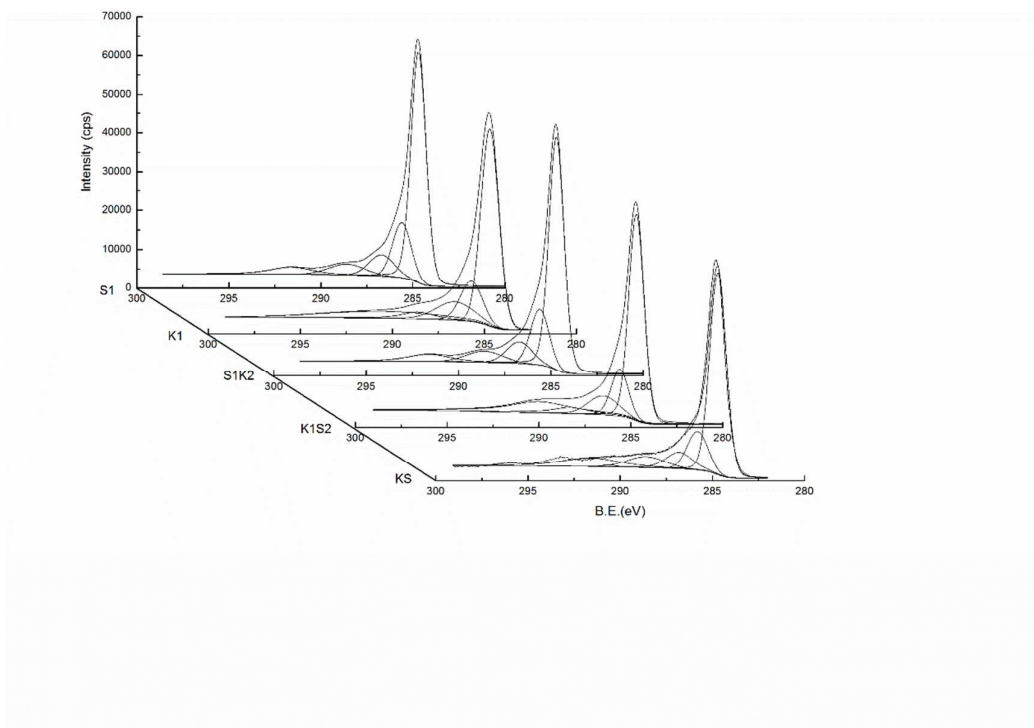
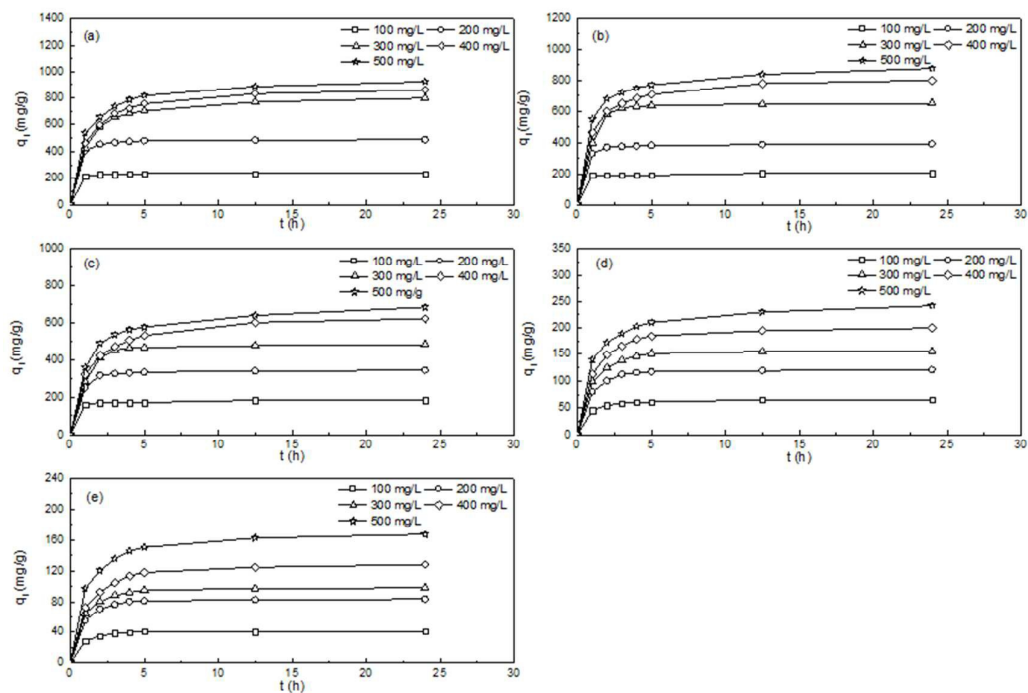Fig. 6. XPS spectra of C1s region of the liquefied wood-based ACFs prepared by different activation methods.

Fig. 7. The variation of adsorption capacity of ACFs with adsorption time at various initial MB concentrations at 25 °C: (a) KS; (b) K1S2; (c) K1; (d) S1; (e) S1K2.
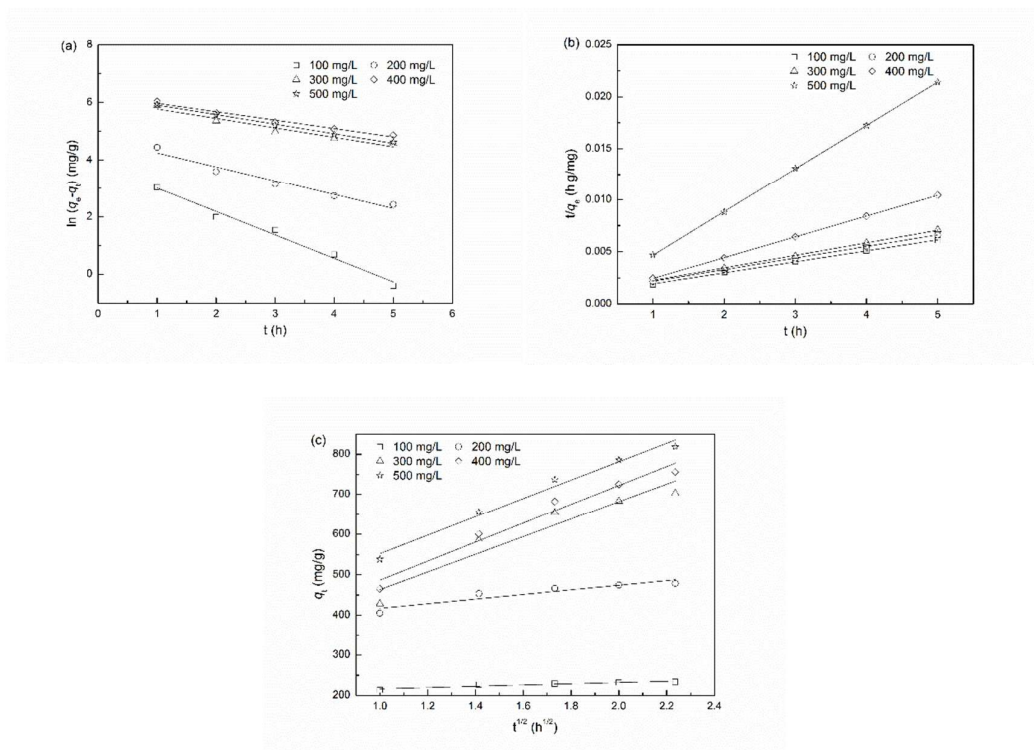
Fig. 8. Kinetic models for adsorption of MB adsorption onto KS at 25 oC. (a) Pesudo-first-order kinetics; (b) Pesudo-second-order kinetics; (c) Intraparticle diffusion model.

Table 1 Pore structural parameters of ACFs from N_2 adsorption isotherms and their adsorption capacity for MB.

Sample	Total surface area[a] (m^2/g)	Total pore volume[b] (cm^3/g)	Micropore volume[c] (cm^3/g)	Mesopore volume[d] (cm^3/g)	Marcopore volume[e] (cm^3/g)	Yield[f] (%)	MB adsorption (mg/g)
S1	1240	0.64	0.38	0.214	0.046	41	242
S1K2	1081	0.558	0.364	0.177	0.017	27	167
K1	545	0.504	0.013	0.41	0.081	76	684
K1S2	1658	1.214	0.49	0.486	0.238	30	877
KS	1651	1.097	0.418	0.521	0.158	26	920

[a] Calculate from the Brunauer-Emmett-Teller (BET) method; [b] Calculate from the N_2 adsorption at a relative pressure of 0.995; [c] Calculate from the V-t method; [d] Calculate from the BJH method; [e] Calculate from the difference between the total pore volume and the sum of micro- and mesopore volume; [f] Base on the weight ratio of ACFs to precursor fibers

Table 2 Elemental compositions (wt%) of ACFs as determined by EDX.and pH_{pzc} value of ACFs.

Sample	Elemental analysis			pH_{pzc}
	C (wt%)	O (wt%)	N (wt%)	
S1	90.7	8.9	0.4	6.2
K1	87.1	12.3	0.6	6.4
S1K2	82.6	16.8	0.6	6.5
K1S2	90.3	9.2	0.5	6.2
KS	89.7	9.8	0.5	6.1

Table 3 Langmuir and Freundlich isotherm model constants and correlation coefficients for adsorption of MB onto KS

Isotherms	Sample	Constants			R^2
			b		
		Q_0 (m/g)	(L/mg)	R_L	
Langmuir:					
$C_e/q_e=1/(Q_0b)+C_e/Q_0$	KS	915.75	1.12	0.0018	0.999
	K1S2	862.34	0.68	0.0029	0.998
	K1	680.33	0.84	0.0024	0.999
	S1K2	158.26	0.77	0.0026	0.998
	S1	234.57	1.03	0.0019	0.999
		K_F (mg/g)	$1/n$		
Freundlich:					
$\log q_e=\log K_F+(1/n)\log C_e$	KS	340.65	0.22		0.891
	K1S2	460.63	0.23		0.785
	K1	283.71	0.26		0.832
	S1K2	65.48	0.28		0.774
	S1	90.26	0.33		0.645

Table 4 Comparison of the pseudo-first-order, pseudo-second-order and intraparticle diffusion model for different initial MB concentrations

Model		Constants				
C_0 (mg/L)		100	200	300	400	500
$q_{e,exp}$ (mg/g)		234.03	489.85	800.26	861.44	922.71
Pseudo-first-order:	$q_{e,cal}$ (mg/g)	45.6	114.18	448.18	527.18	516.98
$\ln(q_e-q_t)=\ln q_e-k_1 t$	k_1 (h^{-1})	0.82	0.49	0.33	0.29	0.33
	R^2	0.984	0.960	0.947	0.983	0.996
	SSE	188.43	374.66	349.76	357.71	402.45
Pseudo-second-order:	$q_{e,cal}$ (mg/g)	238.66	500.75	832.64	899.28	948.77
$t/q_t=1/(k_2 q_e^2)+t/q_e$	k_2 (g/mg h)	0.0014	0.0012	0.0015	0.009	0.038
	R^2	0.999	1.000	0.999	1.000	1.000
	SSE	0.59	2.32	9.11	4.23	11.50
Intraparticle diffusion:	$q_{e,cal}$ (mg/g)	235.57	487.80	739.92	772.25	835.58
$q_t=k_p t^{1/2}$	k_p (mg/g h$^{1/2}$)	15.44	57.31	218.55	235.90	229.28
	R^2	0.877	0.877	0.915	0.968	0.980
	SSE	2.51	9.36	28.93	18.76	13.22